

## A Force Balance Model of Early Spindle Pole Separation in *Drosophila* Embryos

E. N. Cytrynbaum,<sup>\*‡</sup> J. M. Scholey,<sup>\*†</sup> and A. Mogilner<sup>\*‡</sup>

<sup>\*</sup>Center for Genetics and Development, <sup>†</sup>Section of Molecular and Cell Biology, <sup>‡</sup>Department of Mathematics, University of California, Davis, California 95616 USA

**ABSTRACT** The formation and function of the mitotic spindle depends upon force generation by multiple molecular motors and by the dynamics of microtubules, but how these force-generating mechanisms relate to one another is unclear. To address this issue we have modeled the separation of spindle poles as a function of time during the early stages of spindle morphogenesis in *Drosophila* embryos. We propose that the outward forces that drive the separation of the spindle poles depend upon forces exerted by cortical dynein and by microtubule polymerization, and that these forces are antagonized by a C-terminal kinesin, Ncd, which generates an inward force on the poles. We computed the sum of the forces generated by dynein, microtubule polymerization, and Ncd, as a function of the extent of spindle pole separation and solved an equation relating the rate of pole separation to the net force. As a result, we obtained graphs of the time course of spindle pole separation during interphase and prophase that display a reasonable fit to the experimental data for wild-type and motor-inhibited embryos. Among the novel contributions of the model are an explanation of pole separation after simultaneous loss of Ncd and dynein function, and the prediction of a large value for the effective centrosomal drag that is needed to fit the experimental data. The results demonstrate the utility of force balance models for explaining certain mitotic movements because they explain semiquantitatively how the force generators drive a rapid initial burst of pole separation when the net force is great, how pole separation slows down as the force decreases, and how a stable separation of the spindle poles characteristic of the prophase steady state is achieved when the force reaches zero.

### INTRODUCTION

Mitosis, the process by which identical copies of the replicated genome are distributed to the products of each nuclear division, depends upon the action of the mitotic spindle, a self-organizing protein machine based on a network of microtubules (MTs) and a variety of molecular motors (Wittmann et al., 2001; Mitchison and Salmon, 2001). It is known that force generation by MT polymerization-depolymerization and by MT-based motor proteins is important for spindle morphogenesis and for the coordination of chromosome movements during mitosis (Inoue and Salmon, 1995; Sharp et al., 2000b), but how these force generating components are coordinated is unclear.

To improve our understanding of spindle mechanics, we have focused on an investigation of the role of force generating elements (MT dynamics and MT-based motors) in the separation of the spindle poles during spindle morphogenesis in *Drosophila* syncytial blastoderm embryos (Sharp et al., 2000a,b; see *Note added in proof*). *Drosophila* embryonic spindles are amphiastral and thus centrosomes at the spindle poles play a critical role in their organization. Each centrosome, which nucleates a radial array of MTs oriented with their plus ends distal, is duplicated during telophase (Sullivan and Theurkauf, 1995) producing two adjacent daughter centrosomes. They

migrate around the surface of the nuclear envelope during the subsequent interphase and prophase, and come to lie at a predictable spacing characteristic of the prophase steady state (6  $\mu\text{m}$  in cycle 12) that persists for 2–3 minutes (Sharp et al., 2000a,b). After nuclear membrane fenestration there is another pause, the prometaphase steady state, followed by an episode of pole separation that increases pole-pole spacing to 10  $\mu\text{m}$ , characteristic of the metaphase-anaphase A steady state. Finally, after the chromatids have moved to opposite spindle poles, the poles separate further during anaphase B to achieve a final separation of 14  $\mu\text{m}$ .

In this paper, we examine the role of MT-based motor proteins that work by a sliding filament mechanism of the type proposed nearly 30 years ago, in which force-generating enzymes cross-link overlapping spindle MTs and slide them in relation to one another (McIntosh et al., 1969). There exists good biochemical and ultrastructural evidence that the bipolar kinesin, KLP61F acts by such a sliding filament mechanism (Cole et al., 1994; Kashina et al., 1996; Sharp et al., 1999). There also exists evidence that the C-terminal kinesin, Ncd, can cross-link and presumably slide adjacent MTs (McDonald et al., 1990; Karabay and Walker, 1999), and it is plausible to think that dynein anchored on the cell cortex can slide MTs in relation to cortical actin filaments (Dujardin and Vallee, 2002).

These three MT sliding motors, together with MT dynamics, cooperate in the pathway of spindle pole separation by generating complementary and antagonistic forces (Hoyt and Geiser, 1996; Sharp et al., 2000a,b; Brust-Mascher and Scholey, 2002). Specifically, the bipolar kinesin, KLP61F, bound to interpolar MTs, generates MT-MT sliding that

Submitted June 16, 2002, and accepted for publication September 6, 2002.

Address reprint requests to Alexander Mogilner, E-mail: mogilner@math.ucdavis.edu.

pushes the poles apart. This kinesin activity is complemented by minus end directed dynein motors anchored on cortical actin filaments which slide astral MTs relative to the cortex and apply an outward force on the spindle poles. At the same time, Ncd motors (also minus end directed) cross-link interpolar MTs and generate an antagonistic inward force that slides polar MTs past each other thereby pulling the poles together. The basic idea of the multiple motor-dependent transient steady state model is that when the inward and outward forces balance one another, the spindle poles are maintained at a constant spacing (a steady-state structure) and tipping this balance drives the further separation of the spindle poles (Sharp et al., 2000a,b). In this model, specific mitotic movements, such as the repositioning of the spindle poles, do not depend upon the action of individual motors acting alone as previously thought (Gelfand and Scholey, 1992), but instead depend on shifts in the balance of forces generated by multiple MT motors (Sharp et al., 2000b).

Mathematical modeling represents a useful technique for exploring and extending this qualitative model, because it allows one to test how the functional coordination of the properties of individual force generating elements can give rise to the behavior of the ensemble of components that makes up the mitotic spindle. Despite the obvious complexity of the spindle, we reasoned that the very early phases of spindle pole separation during interphase-prophase might be amenable to this approach. At this time, most of the force generating components that are active subsequent to nuclear envelope breakdown, including KLP61F, chromokinesins and kinetochore motors, are sequestered in the nucleus and do not contribute to the process. We hypothesize that outward forces generated by dynein are antagonized by inward Ncd-generated forces in such a way that initially the outward forces exceed the inward forces and the spindle poles move apart. By late prophase the outward and inward forces balance one another and the spindle poles remain at a constant spacing characteristic of the prophase steady state.

Our model of this relatively simple phase of spindle morphogenesis depends upon the assumption that the Ncd mediated inward force is proportional to the degree of overlap of the interpolar MTs whereas the outward dynein force is determined by the geometry of the actin and MT networks adjacent to the nucleus. Roughly speaking, the degree of overlap of the interpolar MTs is proportional to the distance between the poles. Initially, when the poles are close to each other, the polar MT overlap is insignificant and thus the outward (dynein) force exceeds the inward force so that the poles separate. As pole-pole separation increases, the extent of MT overlap increases and thus the inward Ncd-generated force increases, and consequently the rate of pole separation decreases. Eventually, a stable stationary separation is achieved when the inward and outward forces balance each other.

Our qualitative description of spindle pole separation (see Fig. 8 a of Sharp et al. (2000a)) is incomplete because it does not take into account certain key geometrical and mechanical factors that could contribute to spindle pole separation, including, for example, force generation by MT polymerization-depolymerization (Bray, 2001; Inoue and Salmon, 1995; see *Note added in proof*) nor does it explain, in detail, the mechanical stability of the pole's separation in the end of the prophase (the prophase steady state). Quantitative modeling that incorporates MT dynamics as well as motor action can improve our understanding of the mechanistic basis of the stability of the prophase steady state, it may illuminate the spatiotemporal organization of motors and cytoskeleton that is essential for the observed phenomenon, and it can serve as a guide to future experimental work.

In this paper, we model the stability of the steady pole separation using a force balance differential equation. This equation is complemented by equations describing distribution of MTs, motors, and forces. The equation describing pole separation is solved numerically. Comparison of the model's predictions with the results of (Sharp et al., 2000b) provide further support for the multiple motor-dependent transient steady state model (Sharp et al., 2000a) and identify areas of uncertainty where further work will be required to test and refine the model.

## DESCRIPTION OF THE MODEL

### General features of the model

Previously, Sharp et al. (2000a) studied the role of MTs and motors in spindle morphogenesis by monitoring spindle pole separation ( $S$ ) as a function of time ( $t$ ) in control and in motor-inhibited cycle 10-13 *Drosophila* embryos, where  $S$  is the arc length between the poles. Here we focus on the early interphase-prophase period of pole separation that lasts  $\sim 500$  s (See Fig. 1 in Sharp et al., 2000a); we note that a calibration error was found that necessitates that the time scales on the published abscissas be multiplied by a factor of 1.68 and only corrected time values are used throughout the current manuscript). Here we model  $S(t)$  (see Table 1 and Figs. 1 and 2 for definitions of model parameters) based on properties of the force-generating elements (MTs and motors) that are known or can be approximated based on reasonable assumptions. We want to know how well the model fits the corresponding plots of  $S$  versus  $t$  during interphase-prophase from the experiments of Sharp et al. (2000a), and also how a stable separation of the spindle poles is maintained when all the forces balance one another. The mechanical system that separates the spindle poles operates at low values of Reynolds number. Rate of separation is limited by  $0.1 \mu\text{m/s}$ ; characteristic dimension of the spindle is  $10 \mu\text{m}$ . Thus, Reynolds number  $Re = (0.1 \mu\text{m/s} \times 10 \mu\text{m}) / (10^6 \mu\text{m}^2/\text{s}) = 10^{-6}$ , where  $10^6 \mu\text{m}^2/\text{s}$  is kinematic viscosity of water. In this regime, inertial forces are negligible, and the rate of separation is proportional to the tangential force applied to the poles (Purcell, 1977). Here and below the tangential force means the component of the force parallel to the nuclear envelope surface:

$$ds/dt = 2F(S)/\mu. \quad (1)$$

Here  $\mu$  is the coefficient of viscous resistance, and  $F(S)$  is the force acting on each of the spindle poles so that the rate of pole separation is twice the rate of each pole's movement. We note that the velocity of spindle pole separation,  $dS/dt$ , corresponds to the slope of the plot of  $S$  vs.  $t$ , and is maximal when

**TABLE 1 Model parameters**

Symbol	Value	Meaning
$L$	$10 \mu\text{m}$	Radius of the actin cap
$h$	$3 \mu\text{m}$	Depth of the actin furrow around the nucleus
$r_n$	$3.35 \mu\text{m}$	Radius of the nucleus
$r_p$	$0.5 \mu\text{m}$	Radius of the centrosome
$g$	$2 \mu\text{m}$	Distance from the nucleus to the actin cap
$w$	$1 \mu\text{m}$	Width of the actin cap furrow
$\lambda$	$8 \mu\text{m}$	Average MT length
$n_0$	100	Number of astral MTs from a single centrosome
$n_1$	4	Number of interpolar MTs from a single centrosome
$f_1$	$10 \text{ pN}/\mu\text{m}$	Dynein motor force per unit length of MT
$f_2$	$2 \text{ pN}/\mu\text{m}$	Ncd motor force per unit length of MT
$f_3$	$5 \text{ pN}$	MT polymerization stall force
$\mu$	$800 \text{ pN}\cdot\text{s}/\mu\text{m}$	Effective viscous drag coefficient

$F(S)$  is maximal, decreases as  $F(S)$  decreases and falls to zero when  $F(S) = 0$  (the prophase steady state). Thus the solution to differential Eq. 1 is  $S(t)$ , which can be used to generate a plot of  $S$  vs.  $t$  for comparison with the data obtained by Sharp et al. (2000a).

To accomplish this, we first calculate the total force  $F(S)$  as a function of pole separation, where  $F(S) = F_{\text{out}} - F_{\text{in}}$ .  $F_{\text{out}}$  is the outward force due to cortical dynein pulling and interpolar MT polymerization pushing the poles apart, and  $F_{\text{in}}$  is the inward force due to Ncd drawing the poles together. Second, we analyze the function  $F(S)$  to find the stationary spacing of the spindle poles  $S_0$  at the prophase steady state (mathematically,  $S_0$  can be found from the equation  $F(S_0) = 0$ ) and we demonstrate that the derivative of the force with respect to separation distance is negative at this stationary

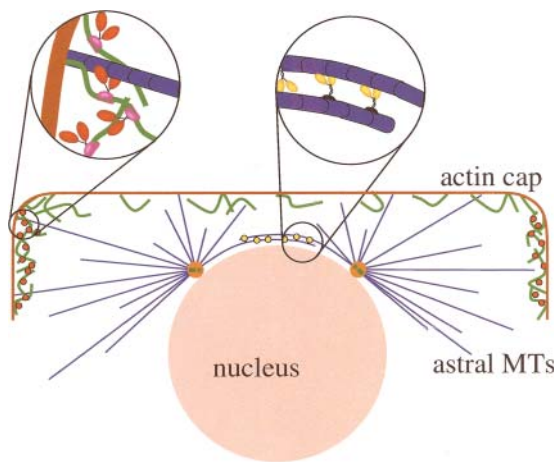


**FIGURE 1** A diagram of the principle structures involved in spindle morphogenesis in interphase-prophase. The nucleus (pink disc) is relatively isolated by the surrounding furrows (brown curve). Along the inner surface of the membrane is a layer of actin (green strands) which binds to the minus end directed motor, dynein (red, see magnified region on the left) through dynactin. MTs (blue lines) extend outward from each of two centrosomes. A few astral MTs interact with dynein on the surface of the actin cap. Interpolar MTs are cross-linked by Ncd motors (yellow, see magnified region on the right).

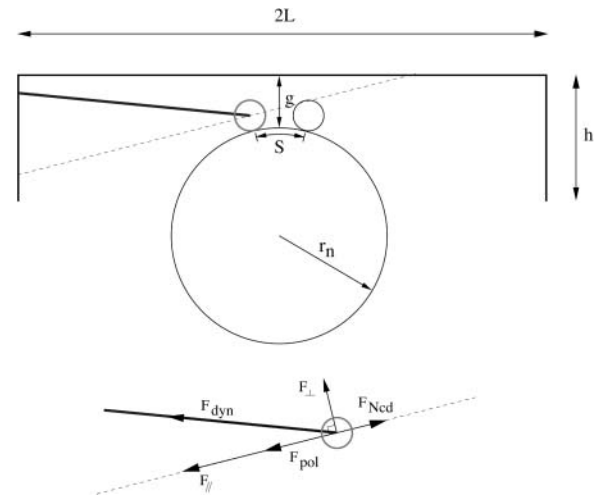


**FIGURE 2** Geometry of the model (cross section).  $S$  is the arclength separation of the centers of the centrosomes,  $L$  is the radius of the inner surface of the cylindrical actin cap,  $h$  is the depth of the furrow, and  $g$  is the distance between the nucleus and the actin cap. In calculating the forces applied to a particular centrosome, we project them onto the tangent plane to the nuclear surface (dashed line). For example, the MT in the top half of the figure exerts a force  $F_{\text{dyn}}$  on one of the centrosomes. This force must be decomposed into components, one perpendicular and one parallel to the nuclear surface. It is the parallel force that contributes to the movement of the centrosome. Once the parallel component is calculated, it can be added to the  $F_{\text{pol}}$  and  $F_{\text{ncd}}$  to find the total driving force.

spacing,  $(dF/dS)(S_0) < 0$ . This means that the spindle is stable once this stationary spacing is attained because fluctuations that separate the poles further are corrected by negative (inward) forces and fluctuations that draw the poles together are compensated by positive (outward) forces. Consequently, the poles are maintained at the distance  $S_0$  from each other, even in the presence of perturbing fluctuations. Finally, we integrate Eq. 1 to find the time course of the pole's separation  $S(t) = \int_0^t (dS/d\tau) d\tau$ . Comparison of values of  $S_0$  and the function  $S(t)$  with experimental results supports the model.

To calculate each of the forces that act on the spindle poles, the spindle environment in the context of the early *Drosophila* embryo must be described in quantitative terms. In doing so, we make a number of simplifying assumptions that are typical of mathematical models. These are described and justified in the following paragraphs.

**Geometrical considerations**

During interphase of cycles 10 through 13, cortical actin is organized into a concentrated network located in the region directly above each nucleus and below the cell membrane. During prophase, this actin cap spreads outward and ingresses down into the cytoplasm between adjacent nuclei (Karr and Alberts, 1986; Sullivan and Theurkauf, 1995; Foe et al., 2000). We idealize the surface of this actin cap as a flat circular area of radius  $L$  above the nucleus and a cylindrical furrow of actin extending down into the cytoplasm around the nucleus with a depth  $h$  (Figs. 1 and 2). The nucleus, a sphere with radius  $r_n$ , maintains a distance  $g$  beneath the center of the actin cap. Throughout the process of spindle pole separation, we assume that this distance and the dimensions of the actin cap remain constant. We also assume that there is a strong force normal to the nuclear surface that holds the centrosomes close to the surface. The origin of this force is unknown because although dynein has been proposed to anchor centrosomes to nuclei in fly embryos (Robinson et al., 1999), no evidence in support of this

hypothesis was obtained in our experiments (Sharp et al., 2000a) and it is equally plausible to think, for example, that centrosomes are constrained to the outer membrane of the nuclear envelope as peripheral protein complexes that are held by lipid anchors. But whatever the identity of this attachment mechanism, it serves to constrain the motion of the separating centrosomes to a trajectory that follows the nuclear surface (Karr and Alberts, 1986). Consequently, it is only the component of the outward forces which is tangential to the nuclear envelope that plays a role in spindle pole separation.

## Organization of astral and interpolar MTs

### Astral MTs

Although we describe the generation of forces in the paragraphs that follow by referring to the behavior of individual MTs, in calculating the forces we assume that MTs can be described by a radial density function, which corresponds to tens to hundreds of MTs that emanate from the centrosome. In defining this function we assume that i) MTs are straight and oriented radially; ii) each centrosome nucleates MTs with a uniform distribution of orientations spanning the hemisphere above the tangent plane to the nuclear surface; iii) the total average number of the astral MTs is constant; and iv) they display an exponential length distribution in accordance with a simple phenomenological model of dynamic instability (Dogterom and Leibler, 1993). We also assume that the dynamics of MTs are fast compared to the movement of spindle poles, based on the fact that the timescales of growth and rapid shrinking of MTs undergoing dynamic instability are of the order of seconds, whereas the timescales of pole separation are of the order of hundreds of seconds (except during the initial rapid burst of pole separation when MT dynamics and pole separation are comparable; see Appendix). Consequently, as a centrosome is pulled along the surface of the nucleus, moving from one position to the next, there is sufficient time for the MT array associated with it to turn over completely and reach a steady-state spatial distribution of lengths.

### Interpolar MT bundle

We assume that a constant total average number of MTs is cross-linked into the interpolar MT bundle, and that the trajectory of the bundle follows the same great circle to which centrosome movement is constrained. In accordance with the dynamic instability model (Dogterom and Leibler, 1993), we assume an exponential length distribution for interpolar MTs as well as astral MTs, and that astral MTs and interpolar MTs have the same average length,  $\lambda$ . The details of the astral and polar MT distributions are given in the Appendix.

## Dynein generated force

In our model, dynein anchored on the cortical actin caps during interphase-prophase exerts an outward force,  $F_{\text{dyn}}(S)$  (Sharp et al., 2000a,b). This force pulls the spindle poles apart by tugging on the astral MTs to which they are anchored. Consider, for example, a single MT extending outward from one of the centrosomes to the encircling actin network (Fig. 2). If it reaches the actin network, actin-bound dynein motors exert an outward force on the centrosome as they try to walk toward the centrosome-bound minus end of the MT. At the surface of the nucleus, the normal component of this force is counterbalanced by strong forces that hold the centrosome close to the nucleus but the component of the force that is tangential to the nuclear surface has the effect of moving the spindle pole along the surface of the nuclear envelope. Our model makes use of the assumption that the number of cortical dynein motors capable of making productive attachments to growing astral MTs is much greater than the number of growing MTs reaching the cortex and thus the concentration of MT plus ends reaching the actin cap is rate limiting in the dynein/MT interaction. This assumption is justified by the fact that only a few tens of MTs reach the actin cap, whereas

there are many more individual dynein motors associated with F-actin. To estimate the force generated by dynein, we also assume that, other than during the initial rapid phase of pole separation, the motors are likely to operate near stall. This assumption is based on the observation that the rates of pole separation,  $\sim 0.01 \mu\text{m/s}$  are much less, than the rates of free movements of the motors,  $\sim 0.1 \mu\text{m/s}$  (McDonald et al., 1990; Gross et al., 2000) and that the motors are slowed by a load-dependent (rather than regulatory) mechanism. (We discuss the situation during the initial phase of rapid separation in the Appendix.) Thus, each motor generates, on average, its stall force,  $\sim 1\text{--}10 \text{ pN}$  (Schmitz et al., 2000; Ashkin et al., 1990). The total force generated by this mechanism is estimated to be equal to the vector sum of the forces generated by all such MTs. The total dynein force,  $F_{\text{dyn}}(S)$  as a function of the arc length between the poles,  $S$ , is computed in the Appendix using geometric formulae and numerical integration and is plotted in Fig. 4.

Our preliminary calculations demonstrated that if dynein is allowed to exert its force on the poles from all regions of the actin cap surface then those forces cannot explain the dynamics of spindle pole separation observed by Sharp et al. (2000a). This is due to a strong restoring force exerted by the dynein in the top circular part of the cap. For this reason, we assume that the concentration of active cortical dynein is higher in the region of the cylindrical furrows of the actin caps (Fig. 1) than in the top of the cap, possibly because actin itself becomes depleted from the top of the cap as it redistributes to the ingressing furrows. Thus we are essentially assuming that no force is exerted on MTs that extend into the top of the cap. Evidence for the lower concentration of actin at the top of the actin cap can be found in (Wam et al., 1984, Fig. 6 *a*; Foe et al., 2000, Fig. 2, row 5, and Fig. 3, row 5; Karr and Alberts, 1986, Fig. 7 *B*).

## Ncd generated force

In our model, Ncd acts on interpolar MT bundles and generates an inward force on the spindle poles,  $F_{\text{ncd}}(S)$ , that varies as a function of spindle pole separation. As the poles move apart, the number of sites on the interpolar MT bundles that become available for productive interactions with Ncd increases. This inward force, which is thought to depend upon the ability of Ncd to cross-link and slide antiparallel interpolar MTs relative to one another (Sharp et al., 2000a), counterbalances the outward forces generated by cortical dynein and MT polymerization (Fig. 1). We assume that there is a sufficiently high concentration of Ncd motors (so that they cover the whole available length of MT fibers (Endow and Komma, 1996)), that they operate near stall and that the force they generate is additive. In the Appendix, we use the length distribution of interpolar MTs to calculate the overlap between antiparallel MTs and integrate over the length of the interpolar MT bundle to find the total Ncd force,  $F_{\text{ncd}}(S)$ , as a function of the arc length between the poles.

## Microtubule polymerization force

In our model, polymerizing interpolar MTs emanating from each pole are capable of exerting an outward force on the opposite pole, and this force,  $F_{\text{pol}}(S)$ , decays with spindle pole separation due to geometric factors. As MTs polymerize, they are capable of pushing any mobile obstacle in the direction of their polymerization (Dogterom and Yurke, 1997; Mogilner and Oster, 1999; van Doorn et al., 2000). Thus, as MTs nucleated at one centrosome run into the other, they should exert a force on it (Fig. 3; see *Note added in proof*). We assume that the poles separate slowly relative to the unencumbered polymerization rate so that the polymerization force produced by a single MT lies close to the polymerization stall force and so is treated as a constant, independent of velocity. The total force due to polymerization will decrease with separation distance for two reasons. First, the density of MTs encountering the other centrosome drops off with separation distance because of the exponentially decreasing length distribution of the fibers and because of the geometric factor (density of MTs crossing a sphere of radius  $R$  centered at the centrosome scales as

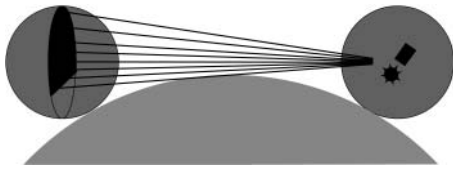


FIGURE 3 Approximating the polymerization force. The centrosome on the right nucleates MTs that run into and get stalled by the centrosome on the left. In estimating the total polymerization force generated by these MTs, we calculate the area of a disc through the middle of the centrosome to approximate the surface area of MT-centrosome interaction. When the centrosomes are sufficiently far apart, the nucleus blocks some of the MTs that would otherwise exert a force. To account for these, a portion of the area of the disc is eliminated according to the relative positions of the centrosomes and the nucleus, as shown in the diagram.

centered at the centrosome scales as  $\sim 1/R^2$ ). Second, as the centrosomes separate, they become hidden from each other by the horizon of the nucleus (Fig. 3). All these factors are taken into account in our calculation of the polymerization force,  $F_{\text{pol}}(S)$ , in the Appendix. We only consider forces generated by polymerization of MT plus ends based on the assumption that the minus ends are relatively inactive. We also assume that the plus ends at the cortex do not generate significant force because MTs at the cortex can depolymerize while cortical dynein reels them in. When experimental data on force generation at the cortex and MT minus ends become available, adjustments to our model will be made to accommodate additional force generators.

### Force scales

Here we make approximate, order-of-magnitude estimates of the essential forces generated by the force generating elements considered in our model based on data gleaned from the micrographs of Karr and Alberts (1986), Sharp et al. (2000a), and Foe et al. (2000). The number of astral MTs associated with each centrosome is  $\sim 100$ . Only  $\sim 10$  of them are long enough and oriented properly to reach the side of the actin cap and generate the outward force. Assuming that the thickness of the actin cap is  $\sim 1 \mu\text{m}$ , and that there are only a few active dynein motors per micron capable of developing a pulling force of the order of a few pN each along the fiber, we can estimate the order of magnitude of the outward force due to dynein as being  $\sim 100$  pN. Similarly, assuming that relatively few MTs are cross-linked into the interpolar bundle, and that only a few Ncd motors per micron are capable of exerting an inward force of the order of a few pN each, we estimate an inward force of  $\sim 100$  pN at a few microns of separation between the poles.

When the separation between the centrosomes is very small, we estimate that a few tens of MTs emanating from one centrosome run into the other one and exert a pushing force. Each one of the nearly stalled fibers develops  $\sim 10$  pN pushing force, so the maximal polymerization force amounts to hundreds of piconewtons. These estimates indicate that all considered forces are of the same order of magnitude, and so they are equally important. The nature of the resistance force developing when the centrosome moves along the nuclear surface is unknown. Both cytoplasmic viscosity and protein friction are likely to play significant roles (Leibler and Huse, 1993). The measurements of (Sharp et al., 2000a) suggest that the maximal rate of pole separation is  $\simeq 0.1 \mu\text{m/s}$ . According to our estimates, this rate is generated by a net outward force on the order of  $\sim 100$  pN. The corresponding drag coefficient has to be  $\sim 1000$  pN·s/ $\mu\text{m}$ . Note, that the viscous drag coefficient of the  $1 \mu\text{m}$  centrosome sphere estimated using Stoke's formula is  $\sim 0.01$  pN·s/ $\mu\text{m}$  (Berg, 1983). Even considering the effective viscosity of the cytoplasm, which is hundreds times greater than the viscosity of water (Marshall et al., 2002) we estimate the drag coefficient to be only  $\sim 10$  pN·s/ $\mu\text{m}$ . However, if we consider the increase in Stoke's

radius due to the radial array of astral MTs associated with each centrosome, this value is increased further. As this aster is very dense, at low Reynolds numbers, its drag is similar to that of a sphere of radius close to the average MT's length,  $\sim 10 \mu\text{m}$ , therefore the estimated drag coefficient is  $\sim 100$  pN·s/ $\mu\text{m}$ . Indeed, the effective drag coefficient would be even higher due to protein friction between the centrosome and nuclear surface.

## RESULTS

### Force balance and stable stationary separation of the spindle poles

The outward forces generated by MT polymerization and cortical dynein and the inward forces generated by Ncd motors are computed in the Appendix and plotted in Fig. 4 as functions of spindle pole separation. The positive and negative values correspond to the out- and inward forces, respectively. All forces are computed for separations  $> 1 \mu\text{m}$  (we consider centrosomes as rigid spheres with radii  $0.5 \mu\text{m}$ , so the separation measured from center to center cannot be  $< 1 \mu\text{m}$ ).

The outward polymerization force decreases rapidly as the separation grows and becomes zero at separations  $> 5 \mu\text{m}$  because of the geometric factors described above. The outward dynein force is smaller than maximal at small separations, because MTs of all orientations can reach all sides of the actin cap, so that the geometric sum of forces is reduced by symmetric forces. Also, only a small area at the sides of the cap is accessible to the MTs because of the steric limitations from the nuclear surface (Fig. 6). As pole separation increases, the outward force also increases, because the horizon of the nucleus blocks the remote half of the actin cap, and because the accessible area at the cap's closer side increases. The local minimum (in the separation dependence) of this force at  $\sim 1.5 \mu\text{m}$  appears because the neighboring centrosome shadows parts of the actin furrows at small separations. At greater separations, the increase in outward force slows, and then starts to decrease as the direction of the resulting force gradually becomes normal to the nuclear surface, and thus its tangential projection decreases.

The inward force generated by the Ncd motors is small when the separation is small, because the extent of overlap between the interpolar MTs, and thus the number of active motors, is proportional to spindle pole separation. This force reaches a maximum at a pole separation of the same order of magnitude as the average length of MTs, and then starts to decrease, because fewer MTs are long enough to overlap at such great distances.

With the experiments of Sharp et al. (2000a) in mind, we express the total tangential force on the centrosome (coming from the vectorial sum of three physical forces) in the form:

$$F(S) = aF_{\text{dyn}}(S) + bF_{\text{ncd}}(S) + F_{\text{pol}}(S). \quad (2)$$

Here  $a$  and  $b$  are dimensionless scale factors determined by the experimental protocol being simulated:

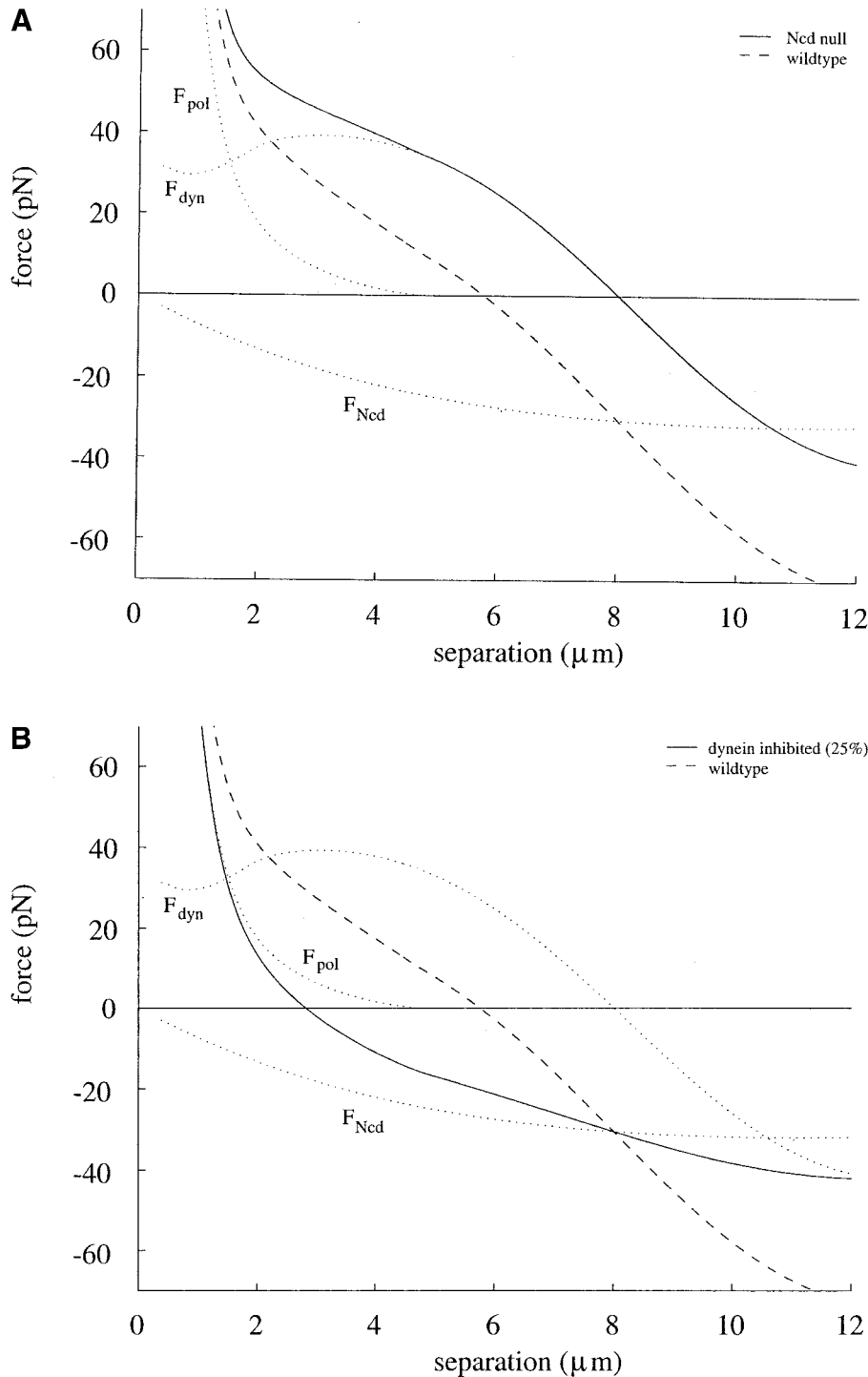


**FIGURE 4** (A) Forces as a function of separation distance. The calculated dynein ( $F_{\text{dyn}}$ ), Ncd ( $F_{\text{ncd}}$ ), and polymerization ( $F_{\text{pol}}$ ) forces are plotted as dotted curves. The total spindle forming force in the wild-type embryo (dashed curve) is calculated by adding all three forces ( $F_{\text{dyn}} + F_{\text{ncd}} + F_{\text{pol}}$ ). Notice a stable steady state ( $F = 0$ ) at  $S \approx 6 \mu\text{m}$ . The Ncd-null embryo (solid curve) is simulated by adding the dynein and polymerization forces ( $F_{\text{dyn}} + F_{\text{pol}}$ ). Eliminating the Ncd force increases the steady-state separation distance to  $\approx 8 \mu\text{m}$ . (B) Same as A except the solid curve shows the total force when dynein is inhibited. In simulating the effect of inhibiting dynein (by exposing the embryo to either p50 dynamitin and anti-DHC), we reduced the calculated dynein force to a fraction of its original amplitude. Here, we plot the force resulting from a reduction in dynein activity to 25% of its original value ( $F = 0.25F_{\text{dyn}} + F_{\text{ncd}} + F_{\text{pol}}$ ). Notice the reduction in steady-state separation distance to  $\approx 3 \mu\text{m}$ . (C) To simulate the combined Ncd-null and dynein inhibited embryo, we eliminate the Ncd force and reduce the dynein force to 25% of its original value. The total force in this case,  $F = 0.25F_{\text{dyn}} + F_{\text{pol}}$ , is shown by the solid curve. In this situation, the steady separation distance is  $\approx 8 \mu\text{m}$  as it was in the Ncd-null case. Also, the amplitude of the force for separation distances between  $3 \mu\text{m}$  and  $8 \mu\text{m}$  is much lower than in the Ncd-null case leading to a much slower separation of the poles, as noted in the experiments (compare Fig. 5, A and C).

1. wild-type force:  $a = b = 1$ ;
2. Ncd-null ( $ca^{\text{nd}}$ ) embryos:  $a = 1$ ,  $b = 0$  (Ncd motors are knocked out, and the corresponding force is zero);
3. dynein inhibited (anti-DHC/p50 dynamitin treated) embryos:  $a = 0.25$  or  $0.5$ ,  $b = 1$  (Dynein motors are inhibited significantly, but it is not known quantitatively to what extent. We assume that 25% or 50% of dynein motors (these fractions give the best fit to the

4. Ncd-null/dynein inhibited embryos:  $a = 0.25$ ,  $b = 0$ .

The forces are plotted superimposed in Fig. 4 A as functions of the separation of the spindle poles. The dashed curve shows the total tangential force as a function of the

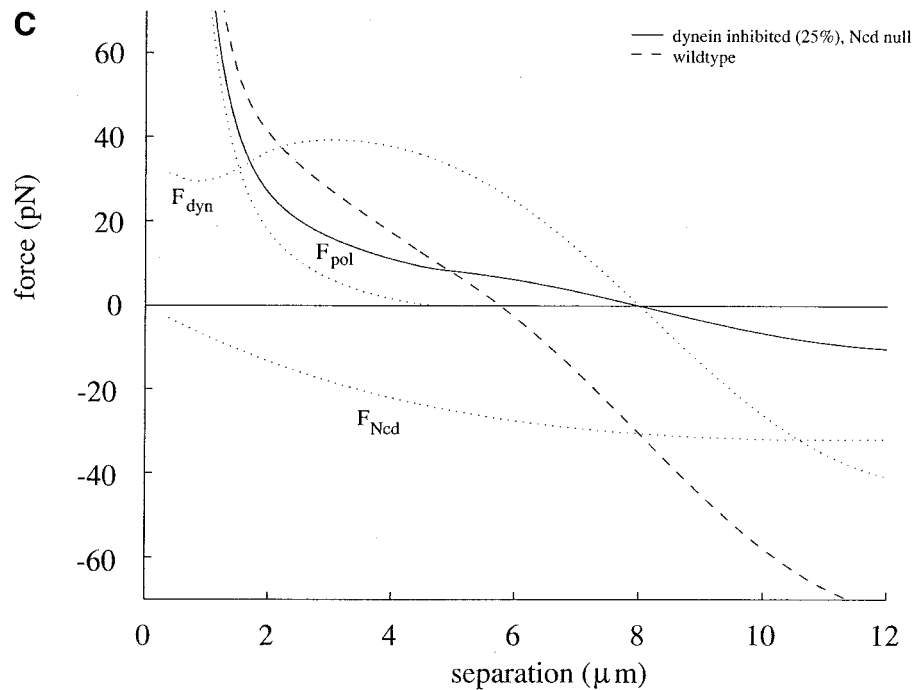


FIGURE 4 Continued.

separation between the poles in the wild-type case. Significantly, the force falls to zero when the spindle poles acquire a spacing of  $S \simeq 6 \mu\text{m}$ . This is the stationary separation that the model predicts and it is stable because at smaller separations the resulting force is positive (outward), and at greater separations it is negative (inward). Thus the model predicts exactly the same stable spacing of the spindle poles as that observed in the experiments of Sharp et al. (2000a).

We have also modeled spindle pole separation under conditions when the dynein and Ncd motors are inhibited. The solid curve (Fig. 4 A) corresponds to the force when Ncd motors are inhibited as in the null mutant and cannot generate an inward force. Then, the theory predicts stationary separations at  $S \simeq 8 \mu\text{m}$ . The solid curve in Fig. 4 B shows the force when 75% of dynein motors are inhibited. Then, the model gives stationary separations at  $S \simeq 3\text{--}4 \mu\text{m}$ . Finally, the solid curve in Fig. 4 C illustrates the force when both Ncd, and 75% of dynein motors are not active. Note that the stationary separation in this case is greater than in the wild-type case; the solid curve is very close to the dashed curve, indicating that the dynamics of the separation in these two cases are very close. These model predictions show a reasonable fit to the data of (Sharp et al., 2000a).

### Dynamic separation of the spindle poles

It was observed that spindle pole separation does not occur at a linear rate, but instead the poles appear to separate in

a roughly hyperbolic manner during interphase-prophase (Sharp et al., 2000a). Our model explains this phenomenon based on the prediction that the total tangential force acting on the poles decreases as the poles separate, and consequently there is a gradual decrease in the rate of pole separation.

To simulate the dynamics of spindle pole separation, we solved numerically Eq. 1 (using Matlab ODE solver *ode45*), where Eq. 2 is used for the total tangential force:

$$\frac{dS}{dt} = \frac{2}{\mu} (aF_{\text{dyn}} + bF_{\text{ncd}} + F_{\text{pol}}). \quad (3)$$

The results of the simulations in four cases corresponding to previously investigated experimental situations are shown in Fig. 5.

There are four different data sets (from Sharp et al., 2000a) to which we fit the results of the model. These correspond to the following four experimental protocols: i) wild type, ii) Ncd null, iii) dynein inhibited, iv) simultaneous Ncd null and dynein inhibited. The parameter values are the same in all four fits and were chosen using the eyeball norm (i. e., no formal optimization algorithm was used).

The wild-type fit is accurate except for the final stage of spindle pole separation. Up until 500 s, there is very clear evidence of a hyperbolic approach to a steady state, but subsequently, poorly understood factors give rise to a perturbation of the steady state as the poles separate to  $7 \mu\text{m}$  (Sharp et al., 2000a). It is possible, for example, that

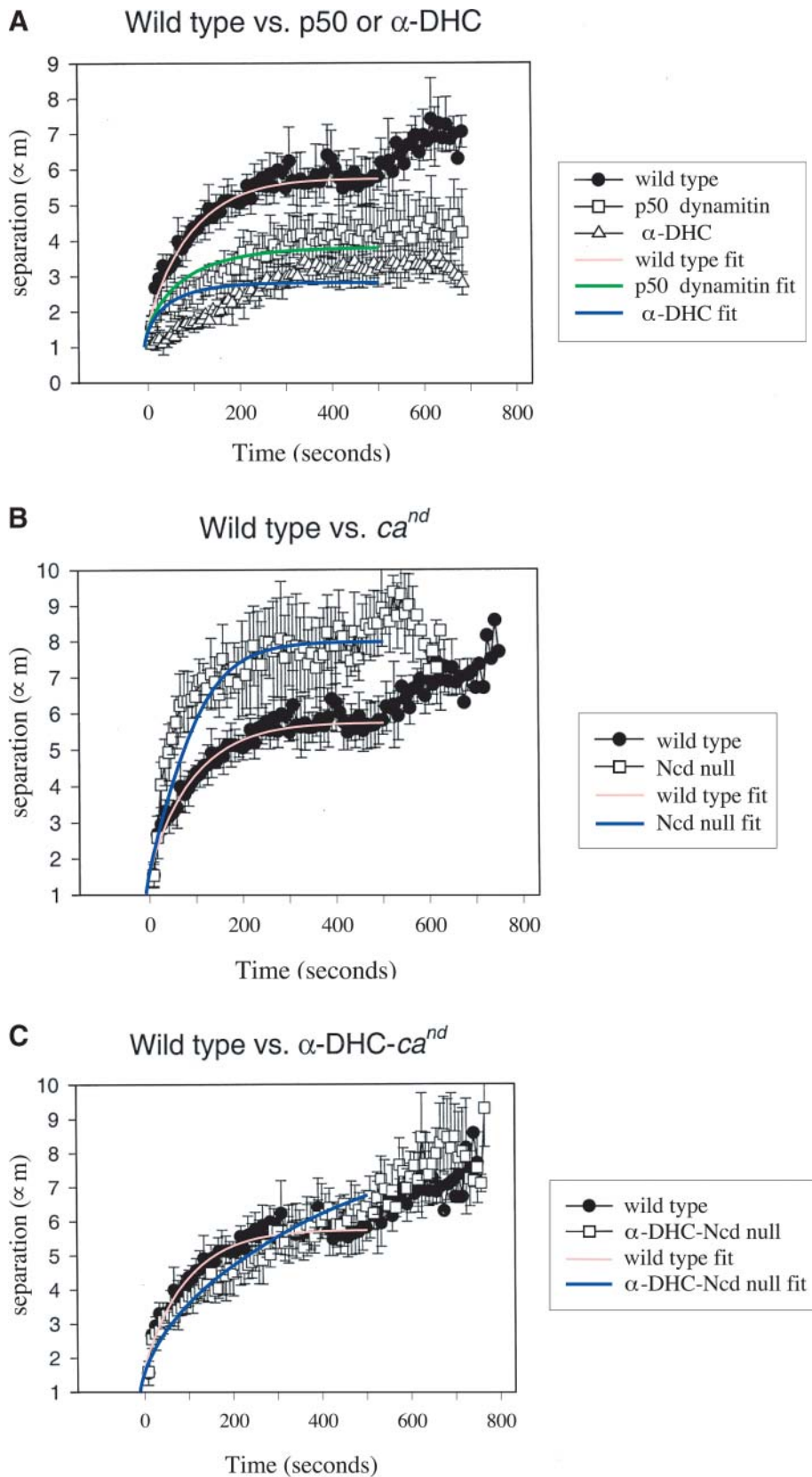


**FIGURE 5** (A) The predicted time course of pole-pole separation fit to the experimental data of Sharp et al. (2000a). The p50 dynamitin data is fit assuming dynein activity is reduced to 50% of the wild-type amplitude and the anti-DHC data is fit assuming a reduction to 25% of the original amplitude. (B) The Ncd-null case. Notice the rapid approach to a steady separation distance of  $\approx 8 \mu\text{m}$ . (C) The dynein inhibited, Ncd-null case. Notice that the slower approach to the same steady state seen in the Ncd-null case ( $\approx 8 \mu\text{m}$ ) gives the impression that the combined dynein inhibited-Ncd-null experiment reestablishes the original separation time course.

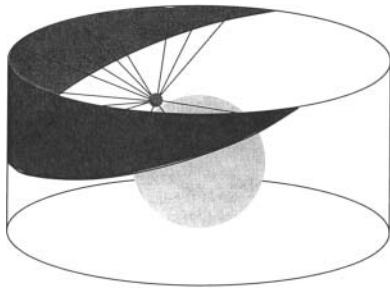


FIGURE 6 The region of dynein-MT interaction. MTs emanating from a centrosome extend only into the half space above the tangent plane to the nucleus because the surface of the nucleus blocks any that extend below this plane. The shadowed region represents the domain in which dynein on the actin cap wall interacts with MTs and is the region over which the dynein force is integrated.

the onset of nuclear envelope breakdown introduces factors that perturb the steady state. As the model only accounts for the factors believed to be involved before the nuclear envelope breaks down, this period is not described in our model but will be a topic of future attention. Also note that the initial separation in the model in the dynein-inhibited case is not as slow as seen in the experiments. It is likely that there is some feature of the early separation that is not captured by the model we propose (see Appendix).

In the case of the Ncd-null mutant, the fit is accurate subsequent to the very early phase. Note that in our model the steady state in this case is entirely determined by the dynein generated force (although in reality other unknown factors could be operating as well). The polymerization force plays a role in the early stage but is eliminated by the time the poles are 5  $\mu\text{m}$  apart.

The fit to the data from the dynein inhibited embryos depends on the fraction of dynein that can generate force. The best fits were obtained when 25% and 50% of dynein remains active in the anti-DHC/p50 dynamitin cases, respectively.

Finally, when both dynein and Ncd are inhibited, the time course of pole separation is very close to the wild-type case. The reason for this phenomenon, as we mentioned above, is that complete inhibition of the Ncd generated inward force is partially compensated by the loss of  $\approx 75\%$  of the dynein outward force, and thus the balance of the outward polymerization force and the residual  $\approx 25\%$  of dynein generated force lies close to the total force balance in the wild-type case. This quantitative result is a very valuable contribution of our model to understanding the early stages of spindle morphogenesis. Quantitative modeling suggests that no additional mechanisms or motor proteins are necessary to explain the experiments with Ncd-null/dynein inhibited mutants.

Generally, the model fits the experimental data of Sharp et al. (2000a) on the time course of spindle pole separation

reasonably well, for both wild-type and motor-inhibited embryos (Fig. 5).

## DISCUSSION

In this work, we demonstrated semiquantitatively that the separation of the spindle poles at the early stages of mitosis could be explained by the antagonistic action of cytoplasmic dynein and MT polymerization generating outward forces and C-terminal kinesin motors generating inward forces. Dynein motors are anchored to the actin cell cortex and by moving toward the minus ends of astral MTs, generate an outward force pulling the spindle poles apart. Ncd motors cross-link antiparallel interpolar MTs and develop an inward force pulling the spindle poles together. During early prophase, this Ncd generated force serves as a brake against the outward force, whereas later these forces balance each other leading to the transiently stable pole separation distance that is characteristic of the prophase steady state. At small distances between the poles, MTs from each pole run into the adjacent centrosome and get stalled creating a polymerization force that enhances the rapid separation of the spindle poles in early prophase.

In our model, the forces due to dynein, Ncd, and MT polymerization are all considered to vary as a function of spindle pole separation (Fig. 4). As the separation grows, the outward force due to MT polymerization decreases because as each pole moves away from the other it interacts with a decreasing number of MTs emanating from the opposite pole, and the inward force due to Ncd initially increases due to an increase in the length of overlapping interpolar MTs with which the motors can interact. At the same time, the outward force due to dynein first increases due to the growth of the accessible area of the pseudocleavage furrows, and then decreases, when the projection of the dynein generated force onto the plane tangent to the nuclear surface diminishes. Significantly, in the wild-type control embryos the forces balance one another when the pole-pole spacing reaches 6  $\mu\text{m}$  as observed experimentally (Sharp et al., 2000a) (Fig. 4 A).

We demonstrated that the experimental observations of Sharp et al. (2000a) placed stringent constraints on the model. To explain the enhanced rate and extent of spindle pole separation observed in Ncd-null mutants, we had to assume that dynein action is largely localized to the lateral ring of the actin cap (the pseudocleavage furrow that lies between and physically separates the spindles). Furthermore, the average length of the interpolar MTs (determined, most likely, by the dynamic instability phenomenon) has to be large enough to equilibrate the outward force in a stable way. The model explains the hyperbolic character of the pole's separation: at small separation, the total force generated by dynein, Ncd, and polymerization is great and directed outward causing fast separation of the centrosomes. Later, at pole-pole spacings of a few microns, the polymerization and dynein forces decrease significantly, whereas the inward

force becomes great due to an increased overlap between long antiparallel interpolar MTs. The sum of these forces is still directed outward, but decreases in magnitude as the poles separate to reach the prophase steady state, at which point spindle pole separation is maintained stably at 6  $\mu\text{m}$ . It is striking how well the model predicts the time course of dynamic spindle pole separation as well as the spacing between the poles at the prophase steady state. The model's value is that it explains not only the behavior of wild-type cells, but also the dynamics of pole separation in mutants. Notably, although the results related to either Ncd, or dynein inhibited cells are intuitively clear, the explanation of the time course of the pole separation when both motors are inhibited requires detailed quantitative analysis. The theoretical explanation for the similarity between the separation kinematics of the wild-type and Ncd-null/dynein inhibited data is one of the important results of the model. Another one is the prediction of the unexpectedly large value of the effective viscous drag coefficient of the centrosome.

Some aspects of cell division have been modeled. These include (but are not limited to) a two-fluid model for cytokinesis (He and Dembo, 1997), a simple model of oscillatory chromosome movement (Joglekar and Hunt, 2002), and a model for chromosome capture in prometaphase (Holy and Leibler, 1994). Self-organization of polymer-motor systems underlying mitotic morphogenesis was modeled in Surrey et al. (2001) and Nedelec (2002); spindle positioning was considered in Grill et al. (2001); and conceptual qualitative models of mitosis are reviewed in Nicklas (1988).

Our model is the first attempt to analyze spindle morphogenesis *in silico*. Using parameter fitting, our model quantitatively explains the data of Sharp et al. (2000a). To test the model's validity without parameter adjustment, the spatial distribution and activity of the molecular motors and the length and angular distribution of MTs have to be measured accurately. In the future, we intend to use various experimental techniques to quantify the geometry and dynamics of the actin cortex, nucleus, and motor distributions. We will also measure the critical characteristics of the MTs involved in this process, such as length and angle distribution, as well as polymerization, catastrophe, and recovery rates. We will use these data to develop a more realistic computational model. The adequacy of this model could be tested by changing MT dynamics in a controlled way and comparing the corresponding theoretical and experimental results. These experiments sound straightforward in principle, but in practice they will be technically challenging yet worthwhile nonetheless.

In its current form, our model is very simple, and thus does not permit the investigation of the role of many possibly important effects. We did not consider the polymerization forces of MTs interacting with the actin cortex (such forces, and their organization by the process of dynamic instability, were investigated theoretically in Holy et al. (1997)). Effects

of the finite rates of MT dynamics on the separation dynamics require a more complex computational approach. Force-velocity relations for motors and MTs are needed for more accurate simulations. One has also to examine the possible effects of cross-linking and motor forces on MT dynamics (Putnam et al., 1998), the effects of MT elasticity forces on a motor's force-velocity characteristics (Gittes et al., 1996), and collective motor effects (Julicher and Prost, 1995). (The motor forces are not necessarily additive.) The structure and dynamics of the actin-rich caps need better examination. The pseudocleavage actin furrows could be created by processes independent of the dynein and Ncd mediated force generation, or they could be the result of, for example, counteraction of dynein power strokes pulling the actin cortex down between the adjacent nuclei. In the latter case, an extended model including coupled dynamics of the MT spindle network and the actin cap's meshwork has to be developed. Our model does not take into account accessory factors, e.g., MT associated proteins, that may modulate MT dynamics and MT-based force generation, or proteins involved in linking MTs to spindle poles or to the cell cortex which could also contribute to spindle pole separation. Finally, independent mechanisms of spindle morphogenesis relying on redundant sets of MT motors, or some novel, yet unidentified, machinery such as a spindle matrix (Scholey et al., 2001; Bloom, 2002) have to be ruled out.

In particular, an important question concerns the precision and robustness of pole separation. During the prophase steady state (as well as those occurring at other stages of mitosis), the fluctuations in the interpolar distance are of the order of only a few percent. According to probabilistic arguments, if, on the average,  $N$  MTs reach the cell cortex, then the relative fluctuations of the outward force and consequently the relative fluctuations of the separation distance between the poles, would be  $\sim 1/\sqrt{N}$ . For example, a 3% fluctuation corresponds to  $N \sim 1000$  MTs, which is far greater than the number of MTs observed. This could indicate that additional control mechanisms maintain the spindle dimensions.

Many other questions remain to be answered before a more adequate and realistic model can be developed. What forces keep the nucleus in place and define its position relative to the cell cortex? What factors/asymmetries determine the plane in which the centrosomes glide along the nuclear surface? What forces keep the centrosomes near the nuclear surface and generate effective resistance to the movement along the surface? What is the nature of MT anchoring at the centrosomes?

Quantitative modeling alone cannot answer these questions. However, it is beginning to and will continue to play an important complementary role to experimental studies in dissecting the complex phenomena of spindle morphogenesis. It would be surprising to us if the details of the current model will not have to be modified in light of more precise determination of experimental parameters. However,

we consider our model to be a valuable and important first step because it provides clear indication that a general force balance model is a useful tool in explaining the dynamics of spindle pole separation.

## APPENDIX

### Geometry

We define a coordinate system  $(x, y, z)$  with the origin located at the center of the nucleus (with vertical axis  $z$ ) such that the great circle on which the centrosomes move is in the  $x$ - $z$  plane. The nucleus occupies a sphere of radius  $r_n$ :  $x^2 + y^2 + z^2 < r_n^2$ . The centrosomes, with radius  $r_p$ , sit on the surface of the nucleus with centers at the points  $\vec{c}_{\pm}(S) = (\pm R \sin(S/2R), 0, R \cos(S/2R))$  where  $R = r_n + r_p$ .

### Astral and polar MTs

The astral MTs associated with one of the centrosomes extend from the center of that centrosome to all points in space above the tangent plane to the nucleus. We use the tangent plane at the point of contact but to simplify the calculation, we approximate this by translating the plane to the center of the centrosome. According to a simple dynamic instability model (Dogterom and Leibler, 1993), the length density of MTs is distributed exponentially,  $\sim e^{-l/\lambda}$ , where  $l$  is MT length, and  $\lambda$  is the mean MT length.  $\lambda$  is determined by the catastrophe and recovery rates and is treated here as a parameter. The total number of MTs emanating from a single centrosome that are longer than  $l$  can be found by integration and is equal to  $n_0 e^{-l/\lambda}$ , where  $n_0$  is the average total number of MTs.

For any distance from the centrosome,  $l$ , the surface density of MTs passing through the point  $\vec{x}$  such that  $l = |\vec{x} - \vec{c}|$  can be found by dividing the total number of MTs of length greater than  $l$  by the surface area of a half sphere of radius  $l$ . This yields the following expression for the density of astral MTs originating from a centrosome at  $\vec{c}$ :

$$A(\vec{x}, \vec{c}) = \frac{n_0}{2\pi l^2} e^{-l/\lambda}, \quad l = |\vec{x} - \vec{c}|. \quad (4)$$

(The factor 2 in the denominator appears because the MTs emanate into half space.)

We use the same exponential length distribution to find the distribution of interpolar MT plus ends. Let  $s$  denote position along the great circle with  $s = 0$  corresponding to the apex of the nucleus. The density of plus ends at a point  $s'$  (with the centrosome at  $\vec{c}_{\pm}(S)$ ) is proportional to  $e^{(\pm s' - S/2)/\lambda}$ . Integrating this expression with respect to  $s'$  from  $s$  to  $\infty$  gives the number of polar MTs originating at  $c_{\pm}$  passing through the point  $s$ :

$$P_{\pm}(s, S) = n_1 e^{(\pm s' - S/2)/\lambda}, \quad (5)$$

where  $n_1$  is the total number of the polar MTs emanating from a single centrosome.

### Dynein generated force

Due to symmetry, we need only to consider the force exerted by dynein motors on one of the two spindle poles. We have assumed that the MT distribution associated with a pole is restricted to the region above the plane tangent to the nucleus at the location of the pole. These MTs interact with dynein bound to the cylindrical wall of actin. The region of the actin wall that is involved in this interaction,  $\Omega$ , is described by the following constraints:

$$\begin{aligned} x \sin(S/2R) + z \cos(S/2R) > R, \quad x^2 + y^2 = L^2, \\ r_n + g > z > r_n + g - h, \end{aligned} \quad (6)$$

where  $L$  is the radius of the cylinder and  $r_n + g$  and  $r_n + g - h$  are the coordinates of the upper and lower edges of the actin wall, respectively. This region is shown in Fig. 6.

In a small region of the actin wall, if the angle between MT fibers and the wall is equal to  $\theta$ , then the surface density of MTs entering the wall in that region is  $A \sin(\theta)$ . Assuming that the thin actin wall has a constant width  $w$ , the length of the MT fibers overlapping with the wall is equal to  $w/\sin(\theta)$ . If a constant number of dynein motors is acting per unit length of fiber, then the force generated by a small patch of dynein around the point  $\vec{x} \in \Omega$  is given by  $f_1 w A(\vec{x}, \vec{c}) \vec{n} d\Omega$  where  $\vec{n} = (\vec{x} - \vec{c})/|\vec{x} - \vec{c}|$  is the normal vector pointing from the centrosome at  $c$  to the patch,  $w$  is the width of the actin wall, and  $f_1$  is the motor's force per unit length. Integrating this vector field over all of  $\Omega$  gives the total force acting on the centrosome,  $\vec{F}_{\text{dyn}}$ . Finally, we are interested in the (properly oriented) component of this vector that lies in the tangent plane at the point  $c$ :

$$\begin{aligned} F_{\text{dyn}} &= \vec{j} \cdot \vec{F}_{\text{dyn}}, \\ \vec{j} &= (\mp \cos(S/2R), 0, \sin(S/2R)), \\ \vec{F}_{\text{dyn}} &= f_1 w \int_{\Omega} A(\vec{x}, \vec{c}) \vec{n} d\Omega. \end{aligned} \quad (7)$$

The choice of  $-$  or  $+$  in front of the cosine function depends on which centrosome we choose to consider ( $-$  for the centrosome with the positive  $x$  coordinate and  $+$  for the centrosome with the negative  $x$  coordinate). The integration and force calculation was done numerically using Matlab for the values of the model parameters given in Table 1 and for values of  $S$  from 0 to  $12 \mu\text{m}$  with increment  $0.1 \mu\text{m}$ .

### Ncd generated force

The force generated by Ncd motors cross-linking two antiparallel MTs with an overlap length  $\delta x$  can be expressed as  $(f_{\text{ncd}}/l_{\text{ncd}})\delta x$ , where  $f_{\text{ncd}}$  is the average force generated by one Ncd motor and  $l_{\text{ncd}}$  is the average length of MT taken up by a single motor. Multiplying this expression by the local density of overlapping MTs and integrating over the length of the interpolar MT bundle gives the total Ncd force,  $F_{\text{ncd}}(S)$  as a function of the arc length between the poles.

The density of overlapping antiparallel MTs at any point is given by the minimum of the densities of MTs extending from the poles. Thus the total force applied to the poles by Ncd is given by

$$\begin{aligned} F_{\text{ncd}} &= f_2 \int_{-S/2}^{S/2} \min(P_+(s, S), P_-(s, S)) ds \\ &= 2f_2 n_1 \lambda e^{-S/2\lambda} (1 - e^{-S/2\lambda}), \end{aligned} \quad (8)$$

where  $f_2$  is the parameter determined by how much force a unit length of two antiparallel MTs covered with Ncd molecules can generate. This formula predicts the separation dependence of the inward force plotted in Fig. 4 for the parameter values given in the Table 1.

### MT polymerization force

As mentioned above, we assume that the polymerization force depends only on the distance between the centrosomes (through the decreasing MT density) and the centrosomal surface area exposed to the growing MTs. As a further simplification, using the fact that the centrosome is relatively small, we treat the centrosome as a flat upright disk and calculate the surface area of the exposed region of that disk. This exposed area, on which MTs extending from the other centrosome apply their polymerization force, is a full disk for sufficiently small separation distances but soon becomes limited by the horizon of the nucleus (whose projection onto the disk is assumed to be flat to simplify the calculation). At some larger separation distance, the

centrosomes set completely relative to one another and are no longer in the way of polymerizing MTs.

The polymerization force can be written as

$$F_{\text{pol}} = f_3 n_0 \alpha \frac{\exp(-S/\lambda)}{4\pi S^2}, \quad (9)$$

where  $\alpha$  is the exposed area of the disk and can be calculated using the formula

$$\alpha = r_p^2 \times \left( \sin^{-1}((a - r_p)/r_p) + \pi/2 \right) + (a - r_p) \sqrt{r_p^2 - (a - r_p)^2}, \quad (10)$$

where  $a$  is the length of the yellow line segment in Fig. 3. In this formula,  $f_3$  is the polymerization stall force for an MT fiber, and  $n_0$  is the total number of the astral MTs. The functional dependence of  $a$  on  $S$  is a straightforward geometric calculation. The force calculation was done numerically using Matlab for values of  $S$  from 0 to 12  $\mu\text{m}$  with increment 0.1  $\mu\text{m}$ .

### Initial rapid phase of pole separation

Initially, when the poles are very close together, the total force arises predominantly from the MT polymerization force and dynein force,  $F(S) \approx F_{\text{pol}}(S) + F_{\text{dyn}}(S)$  (see Fig. 4). This force is very large,  $\approx 100$  pN, and the rate of the pole's separation is fast,  $F/\mu \sim 0.1$   $\mu\text{m}/\text{s}$ . This rate is comparable to the rate of free movement of molecular motors, and the effect of the movement on the motor generated forces cannot be neglected. To understand this effect, let us approximate the force-velocity relation for dynein and MT polymerization by the following linear functions:

$$F_{\text{pol}}(S) = F_{\text{pol}}^0(S) \left( 1 - \frac{v}{V_p} \right), \quad F_{\text{dyn}}(S) = F_{\text{dyn}}^0(S) \left( 1 - \frac{v}{2V_d} \right). \quad (11)$$

Here  $F_{\text{pol}}^0(S)$  and  $F_{\text{dyn}}^0(S)$  are the stall forces of MT polymerization and dynein respectively,  $V_p$  is the free polymerization rate,  $V_d$  is the rate of free movement of dynein motor, and  $v$  is the rate of pole separation. Then, the rate of separation can be found from Eq. 1 as

$$v = \frac{2}{\mu} \left( F_{\text{pol}}^0(S) \left( 1 - \frac{v}{V_p} \right) + F_{\text{dyn}}^0(S) \left( 1 - \frac{v}{2V_d} \right) \right). \quad (12)$$

Solving this algebraic equation, we find:

$$v = \frac{2(F_{\text{pol}}^0(S) + F_{\text{dyn}}^0(S))}{\mu \left( 1 + \frac{2F_{\text{pol}}^0(S)}{\mu V_p} + \frac{F_{\text{dyn}}^0(S)}{\mu V_p} \right)}. \quad (13)$$

In comparison, when the effect of movement on the force generation is ignored, the formula for the separation rate is:

$$v = \frac{2(F_{\text{pol}}^0(S) + F_{\text{dyn}}^0(S))}{\mu}. \quad (14)$$

Comparing these two equations shows that when the separation is greater than  $\approx 3\text{--}4$   $\mu\text{m}$ , the total force decreases enough so that the terms  $2F_{\text{pol}}^0(S)/\mu V_p \ll 1$ ,  $F_{\text{dyn}}^0(S)/\mu V_p \ll 1$  are very small and negligible, assuming that  $V_p \sim V_d \sim 0.2$   $\mu\text{m}/\text{s}$ . Then, our assumption in this paper that all forces are constant and equal to corresponding stall forces is a very good approximation. However, at small separations, these terms are not too small and decrease the initial rate of separation.

This effect may explain the discrepancy between theoretical curves and experimental data at the initial stage of the separation in Fig. 5. In addition, our assumption was that MT turnover is much faster than the motion of the poles at this stage. In fact, the MT dynamics and pole separation are characterized by the same timescales in this situation. More detailed

stochastic modeling will be necessary to examine the initial stage of the separation.

### Model parameters

The model parameters used in the calculations are listed in Table 1. Geometric parameters  $L, h, r_n, r_p, g, w$  are gleaned from the micrographs published in Karr and Alberts (1986), Sharp et al. (2000a), and Foe et al. (2000). Parameters  $\lambda$  and  $n_0$  are of the same order of magnitude as the corresponding values cited in the literature (Bray, 2001; Inoue and Salmon, 1995; Mitchison and Salmon, 2001; Wittmann et al., 2001). The parameter  $n_1$  was selected as being  $n_1 = 4$ , which lies within the range measured in Sharp et al. (1999b). One dynein motor generates a force  $\sim 1\text{--}10$  pN (Schmitz et al., 2000; Ashkin et al., 1990). We chose the value of parameter  $f_1$  assuming that there are a few dynein motors per micron across the actin cap. The force of MT polymerization near stall,  $f_3$ , is chosen to have the same magnitude as measurements (Dogterom and Yurke, 1997) and theory (Mogilner and Oster, 1999; vanDoorn et al., 2000) predict. There are no data on the force generated by Ncd motors. We chose the relatively small value of parameter  $f_2$  assuming that there are a few motors per micron in the interpolar MT bundle and that each such motor generates a force a few times lower than that of kinesin (a few pN, see Schnitzer et al. (2000)) due to the similar structure of kinesin and Ncd and the low duty ratio of Ncd. There are no data on the effective viscous drag coefficient of the centrosome and its associated MT aster. The value listed in Table 1 is chosen from the best fits to the experimental data of Sharp et al. (2000a) (see also estimates earlier in the paper).

### NOTE ADDED IN PROOF

The qualitative model of Sharp et al. (2000a,b) has now been modified to incorporate force generation due to MT dynamics (Brust-Mascher, I., and J.M. Scholey, 2002. Microtubule flux and sliding in mitotic spindles of *Drosophila* embryos. *Mol. Biol. Cell.* 13:3967–3975). While the study does not address early mitotic events, it reveals that a switch from MT flux to MT sliding at anaphase B onset allows pushing forces exerted by polymerizing interpolar MTs to contribute to the outward forces acting on spindle poles.

We thank T. Harris for help at the earlier stages of this work and Drs. G. Civelekoglu and I. Brust-Mascher for useful suggestions.

This project was proposed and supported by National Institutes of Health (grant GM55507-04 to J.M.S.). A.M. and E.C. are also supported by grants from the National Science Foundation (Award DMS-1097746 to A.M.). E.C. is supported by a fellowship from the Burroughs Wellcome Fund through the Program in Mathematics and Molecular Biology.

### REFERENCES

- Ashkin, A., K. Schutze, J. M. Dziedzic, U. Euteneuer, and M. Schliwa. 1990. Force generation of organelle transport measured *in vivo* by an infrared laser trap. *Nature*. 348:346–348.
- Berg, H. C. 1983. *Random Walks in Biology*. Princeton Univ. Press, Princeton
- Bloom, K. 2002. Yeast weighs in on the elusive spindle matrix: new filaments in the nucleus. *Proc. Natl. Acad. Sci. USA*. 99:4757–4759.
- Bray, D. 2001. *Cell Movements: From Molecules to Motility*. Garland Publishing, New York
- Cole, D. G., W. M. Saxton, K. B. Sheehan, and J. M. Scholey. 1994. A 'slow' homotetrameric kinesin-related motor protein purified from *Drosophila* embryos. *J. Biol. Chem.* 269:22913–22916.

- Dogterom, M., and S. Leibler. 1993. Physical aspects of the growth and regulation of microtubule structures. *Phys. Rev. Lett.* 70:1347–1350.
- Dogterom, M., and B. Yurke. 1997. Measurement of the force-velocity relation for growing microtubules. *Science*. 278:856–860.
- Dujardin, D. L., and R. B. Vallee. 2002. Dynein at the cortex. *Curr. Opin. Cell Biol.* 14:44–49.
- Endow, S. A., and D. J. Komma. 1996. Centrosome and spindle function of the *Drosophila* Ncd microtubule motor visualized in live embryos using Ncd-GFP fusion proteins. *J. Cell Sci.* 109:2429–2442.
- Foe, V. E., C. M. Field, and G. M. Odell. 2000. Microtubules and mitotic cycle phase modulate spatiotemporal distributions of F-actin and myosin II in *Drosophila* syncytial blastoderm embryos. *Development*. 127:1767–1787.
- Gelfand, V. I., and J. M. Scholey. 1992. Every motion has its motor. *Nature*. 359:480–482.
- Gittes, F., E. Meyhofer, S. Baek, and J. Howard. 1996. Directional loading of the kinesin motor molecule as it buckles a microtubule. *Biophys. J.* 70:418–429.
- Grill, S. W., P. Gonczy, E. H. Stelzer, and A. A. Hyman. 2001. Polarity controls forces governing asymmetric spindle positioning in the *Caenorhabditis elegans* embryo. *Nature*. 409:630–633.
- Gross, S. P., M. A. Welte, S. M. Block, and E. F. Wieschaus. 2000. Dynein-mediated cargo transport *in vivo*. *J. Cell Biol.* 148:945–956.
- He, X., and M. Dembo. 1997. On the mechanics of the first cleavage division of the sea urchin egg. *Exp. Cell Res.* 15:252–273.
- Holy, T. E., and S. Leibler. 1994. Dynamic instability of microtubules as an efficient way to search in space. *Proc. Natl. Acad. Sci. USA*. 91:5682–5685.
- Holy, T. E., M. Dogterom, B. Yurke, and S. Leibler. 1997. Assembly and positioning of microtubule asters in microfabricated chambers. *Proc. Natl. Acad. Sci. USA*. 94:6228–6231.
- Hoyt, M. A., and J. R. Geiser. 1996. Genetic analysis of the mitotic spindle. *Annu. Rev. Genet.* 30:7–33.
- Inoue, S., and E. D. Salmon. 1995. Force generation by microtubule assembly/disassembly in mitosis and related movements. *Mol. Biol. Cell*. 6:1619–1640.
- Joglekar, A. P., and A. J. Hunt. 2002. A simple, mechanistic model for directional instability during mitotic chromosome movements. *Biophys. J.* 83:42–58.
- Julicher, F., and J. Prost. 1995. Cooperative molecular motors. *Phys. Rev. Lett.* 75:2618–2621.
- Karabay, A., and R. A. Walker. 1999. Identification of microtubule binding sites in the Ncd tail domain. *Biochemistry*. 38:1838–1849.
- Karr, T. L., and B. M. Alberts. 1986. Organization of the cytoskeleton in early *Drosophila* embryos. *J. Cell Biol.* 102:1494–1509.
- Kashina, A. S., R. J. Baskin, D. G. Cole, K. P. Wedaman, W. M. Saxton, and J. M. Scholey. 1996. A bipolar kinesin. *Nature*. 379:270–272.
- Leibler, S., and D. A. Huse. 1993. Porters versus rowers: a unified stochastic model of motor proteins. *J. Cell Biol.* 121:1357–1368.
- Marshall, W. F., J. F. Marko, D. A. Agard, and J. W. Sedat. 2002. Chromosome elasticity and mitotic polar ejection force measured in living *Drosophila* embryos by four-dimensional microscopy-based motion analysis. *Curr. Biol.* 11:569–578.
- McDonald, H. B., R. J. Stewart, and L. S. Goldstein. 1990. The kinesin-like ncd protein of *Drosophila* is a minus end-directed microtubule motor. *Cell*. 63:1159–1165.
- McIntosh, J. R., P. K. Hepler, and D. G. VanWise. 1969. Model for mitosis. *Nature*. 224:659–663.
- Mitchison, T. J., and E. D. Salmon. 2001. Mitosis: a history of division. *Nat. Cell Biol.* 3:E17–E21.
- Mogilner, A., and G. Oster. 1999. The polymerization ratchet model explains the force-velocity relation for growing microtubules. *Eur. Biophys. J.* 28:235–242.
- Nedelec, F. 2002. Computer simulations reveal motor properties generating stable antiparallel microtubule interactions. *J. Cell Biol.* 158:1005–1015.
- Nicklas, R. B. 1988. The forces that move chromosomes in mitosis. *Annu. Rev. Biophys. Chem.* 17:431–449.
- Purcell, E. 1977. Life at low Reynolds number. *Amer. J. Physics*. 45:3–11.
- Putnam, A. J., J. J. Cunningham, R. G. Dennis, J. J. Linderman, and D. J. Mooney. 1998. Microtubule assembly is regulated by externally applied strain in cultured smooth muscle cells. *J. Cell Sci.* 111:3379–3387.
- Robinson, J. T., E. J. Wojcik, M. A. Sanders, M. McGrail, and T. S. Hays. 1999. Cytoplasmic dynein is required for the nuclear attachment and migration of centrosomes during mitosis in *Drosophila*. *J. Cell Biol.* 146:597–608.
- Scholey, J. M., G. C. Rogers, and D. J. Sharp. 2001. Mitosis, microtubules, and the matrix. *J. Cell Biol.* 154:261–266.
- Sharp, D. J., K. L. McDonald, H. M. Brown, H. J. Matthies, C. Walczak, R. D. Vale, T. J. Mitchison, and J. M. Scholey. 1999. The bipolar kinesin, KLP61F, cross-links microtubules within interpolar microtubule bundles of *Drosophila* embryonic mitotic spindles. *J. Cell Biol.* 144:125–138.
- Sharp, D. J., H. M. Brown, M. Kwon, G. C. Rogers, G. Holland, and J. M. Scholey. 2000a. Functional coordination of three mitotic motors in *Drosophila* embryos. *Mol. Biol. Cell*. 11:241–253.
- Sharp, D. J., G. C. Rogers, and J. M. Scholey. 2000b. Microtubule motors in mitosis. *Nature*. 407:41–47.
- Schmitz, K. A., D. L. Holcomb-Wygle, D. J. Oberski, and C. B. Lindemann. 2000. Measurement of the force produced by an intact bull sperm flagellum in isometric arrest and estimation of the dynein stall force. *Biophys. J.* 79:468–478.
- Schnitzer, M. J., K. Visscher, and S. M. Block. 2000. Force production by single kinesin motors. *Nat. Cell Biol.* 2:718–723.
- Sullivan, W., and W. E. Theurkauf. 1995. The cytoskeleton and morphogenesis of the early *Drosophila* embryo. *Curr. Opin. Cell Biol.* 7:18–22.
- Surrey, T., F. Nedelec, S. Leibler, and E. Karsenti. 2001. Physical properties determining self-organization of motors and microtubules. *Science*. 292:1167–1171.
- van Doorn, G. S., C. Tanase, B. M. Mulder, and M. Dogterom. 2000. On the stall force for growing microtubules. *Eur. Biophys. J.* 29:2–6.
- Warn, R. M., R. Magrath, and S. Webb. 1984. Distribution of F-actin during cleavage of the *Drosophila* syncytial blastoderm. *J. Cell Biol.* 98:156–162.
- Wittmann, T., A. Hyman, and A. Desai. 2001. The spindle: a dynamic assembly of microtubules and motors. *Nat. Cell Biol.* 3:E28–E34.